Few-Mode Geometric Description of a Driven-Dissipative Phase Transition in an Open Quantum System

Dmitry O. Krimer[1,*] and Mikhail Pletyukhov[2,†]
[1]Institute for Theoretical Physics, Vienna University of Technology (TU Wien), Wiedner Hauptstraße 8-10/136, A–1040 Vienna, Austria, EU
[2]Institute for Theory of Statistical Physics, RWTH Aachen University, 52056 Aachen, Germany, EU

(Received 30 July 2018; revised manuscript received 15 December 2018; published 13 September 2019)

By example of the nonlinear Kerr mode driven by a laser, we show that hysteresis phenomena in systems featuring a driven-dissipative phase transition can be accurately described in terms of just two collective, dissipative Liouvillian eigenmodes. The key quantities are just two components of a non-Abelian geometric connection, even though a single parameter is driven. This powerful geometric approach considerably simplifies the description of driven-dissipative phase transitions, extending the range of computationally accessible parameter regimes, and providing a new starting point for both experimental studies and analytical insights.

DOI: 10.1103/PhysRevLett.123.110604

Geometric effects manifest themselves in various fields of physics. Being very compact and elegant, a geometric formulation of a system's dynamics also provides a deeper insight by revealing the physical redundancy in the description and paves the way to a topological classification of those properties that remain stable under eventual external perturbations. In closed quantum systems, the most prominent example of a geometric effect is given by the Berry's phase [1], which is accumulated by a system's wave function along with a trivial dynamical phase during an adiabatic cyclic evolution of the system's parameters. Its emergence relies on the gauge freedom in the choice of the wave function's phase. Physically, this is just the coordinate system choice for a transverse spin driven by a rotating magnetic field [2]. Geometrically, it is interpreted as a holonomy effect of the parallel transport in a specific fiber bundle [3]. The Berry connection form and the associated Chern number have become important tools for classifying ground state properties of topological insulators and superconductors [4–7], skyrmionic spin textures [8–10], and topological photonic [11–13] and optomechanical crystals [14,15].

In open systems, the question about a possible geometric description of a system's dynamics is more subtle, since it is governed by a master equation for the system's reduced density matrix, in which the phase gauge freedom seems to disappear at first sight. Sarandy and Lidar [16,17] developed a formal approach valid for slowly varying Lindblad superoperators when the time evolution of the density matrix can be represented in terms of independently evolving Jordan blocks associated with degenerated eigenvalues. They also treated the time-local master equation in analogy by the Schrödinger equation for closed systems. However, a direct transfer of closed system insights is generically obstructed by the dissipative character of open system dynamics, which is reflected in properties of the Liouvillian supermatrix. First, it is not Hermitian, which implies that, in general, its left and right eigenvectors are not related to each other by the Hermitian conjugation, even though they correspond to the same (complex-valued) eigenvalue. Second, the Liouvillian supermatrix possesses a (usually nondegenerate) zero eigenvalue, whose right eigenvector corresponds to a unique steady state, and the left one is independent of system parameters, ensuring the trace conservation during the time evolution. Hence, a gauge freedom in the steady state is absent, and an observation of geometric effects, in close analogy to closed systems, is impossible in the steady state [18].

There are, however, other possibilities to retrieve geometric structures in open system dynamics. For example, they can emerge in the system's response functions [19,20] or in observable quantities like, e.g., a pumped charge through a quantum dot [21]; see Ref. [18] for a review of different approaches to the geometric description of open systems and the related effects. Moreover, dissipation can also serve as a powerful resource for generating topologically protected edge states [22] or it can lead to nonadiabatic dynamics upon encircling of a topologically nontrivial exceptional point [23,24]. In this context, it is desirable to understand conditions under which geometric effects can arise in open systems.

In this Letter, we demonstrate how the Sarandy-Lidar geometric connection arises in a more general context of open quantum systems undergoing the driven-dissipative phase transition (DPT) [25] and having no exact degeneracy. As it will be demonstrated later, this connection is clearly manifested in experimentally measurable quantities. We study a basic open quantum system, the so-called Kerr

 © 2019 American Physical Society

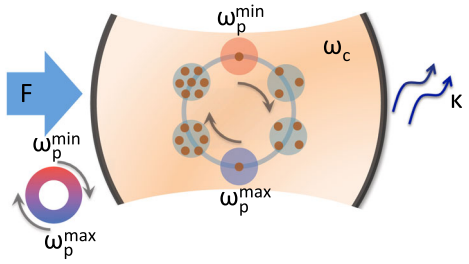

FIG. 1. Single-mode cavity (frequency ω_c, loss rate κ) pumped by a laser field (amplitude F, frequency ω_p). Hysteretic behavior of the cavity occupation number n under a cyclic sweeping of $\delta = \omega_p - \omega_c$ is sketched by brown symbols inside circles. The red and blue color map illustrates the sweeping range $\omega_p^{\min} \le \omega_p \le \omega_p^{\max}$.

nonlinearity model [26], and show that the geometric description is adequate to experimental protocols in which a characteristic timescale t_c of a parameter change is comparable to the lifetime of metastable states present in this system. The importance of metastable states in the understanding of DPT has been recently realized in Refs. [27–29]. Here we establish the powerful approach in which the metastable dynamics can be efficiently treated in terms of just two Liouvillian modes and two components of the Sarandy-Lidar geometric connection, despite the fact that the dynamics is emphatically strongly nonadiabatic relative to the smallest internal timescale generated by DPT. The gauge freedom in this context is unrelated to phase factors being provided instead by rescaling of the lengths of the Liouvillian mode vectors [18]. The corresponding holonomy effect results in nonzero hysteresis areas in parametric dependence of observable quantities. We argue that our description is generally applicable to all open quantum systems featuring metastable dynamics near DPT and that it sheds new light on the relation between multivalued solutions of nonlinear semiclassical (mean-field) equations of motion [30–34] and the linear master equation with a unique parametric solution for the density matrix.

We exemplify our idea by considering the Kerr nonlinearity model (see Fig. 1), which consists of a weakly anharmonic ($|U| \ll \omega_c$), high-quality ($\kappa \ll \omega_c$) single-mode cavity pumped by a strong ($F \gg \kappa$) and possibly off-resonant laser field (detuning $\delta = \omega_p - \omega_c \neq 0$). Here U is the strength of the Kerr self-interaction of the cavity photons, ω_c and ω_p are the cavity and pump frequencies, κ is the cavity loss rate, and F is the laser field amplitude. The system's dynamics is governed by the Lindblad master equation $\dot{\rho}(t) = -i[\mathcal{H}, \rho(t)] + \kappa \mathcal{D}[b]\rho(t) \equiv -i\mathcal{L}\rho(t)$ for the cavity reduced density matrix $\rho(t)$, which is expressed in the rotating frame in terms of the quantum Hamiltonian $\mathcal{H} = -\delta b^\dagger b + (U/2) b^{\dagger 2} b^2 + F(b + b^\dagger)$ and the dissipative superoperator $\mathcal{D}[b]\rho(t) = b\rho b^\dagger - \frac{1}{2} b^\dagger b \rho - \frac{1}{2} \rho b^\dagger b$. Here $b^\dagger$ and b are the bosonic creation and annihilation operators of the cavity photons.

Vectorizing $\rho(t)$, one can find the steady state solution $|\rho_{\rm ss}) = \lim_{t\to\infty} |\rho(t))$ from the linear equation $\mathcal{L}|\rho_{\rm ss}) = 0$, where $\mathcal{L}$ is the Liouvillian supermatrix, and the Dirac-like bra $(\bullet|$ and ket $|\bullet)$ notations for the Liouvillian left and right eigenmode vectors are introduced. For the cases of interest, the Liouvillian supermatrix possesses a zero eigenvalue, and the steady state solution is unique and independent of initial conditions. The nonzero Liouvillian eigenvalues $\lambda_q = \omega_q - i\gamma_q$ labeled by $q = 1, 2, \ldots$, which result from the left $(\bar{\rho}^q|\mathcal{L} = \lambda_q (\bar{\rho}^q|$ and right $\mathcal{L}|\rho^q) = \lambda_q |\rho^q)$ eigenvalue problems, govern the system's dynamics $|\rho(t)) = |\rho^0) + \sum_{q\neq 0} |\rho^q) e^{-i\lambda_q t} (\bar{\rho}^q|\rho(t=0))$ towards the steady state $|\rho_{\rm ss}) \equiv |\rho^0)$. Here ω_q are the oscillation frequencies and $\gamma_q > 0$ are the relaxation rates. In the following, we order eigenvalues λ_q according to the increasing value of γ_q (i.e., λ_1 has the smallest value of $-{\rm Im}\lambda_1 = \gamma_1$). Left and right eigenvectors obey the biorthogonality relation $(\bar{\rho}^{q'}|\rho^q) = \delta_{q'q}$, where $(\bar{\rho}^{q'}|\rho^q) = {\rm tr}[(\bar{\rho}^{q'})^\dagger \rho^q]$ is the Hilbert-Schmidt scalar product. The left eigenvector belonging to the zero eigenvalue is independent of the system parameters and guarantees the trace preservation $(\bar{\rho}^0|\rho(t)) = {\rm tr}[\rho(t)] = 1$ (biorthogonality relation).

At certain parameter values, the Liouvillian spectrum $\{\lambda_q | q = 0, 1, \ldots\}$ undergoes a nearly closing of the dissipative gap [35]: γ_1 becomes vanishingly small as compared to κ, though remaining finite; see Fig. 2(a) for illustration. (Note that the gap is completely closed only in the effective thermodynamic limit featuring the DPT [29,36].) The system enters the regime of the critical slowing-down characterized by the presence of long-lived metastable states [27]. At the same time, the steady mean-field solution, $|\beta_{ss}|^2 = |\langle b \rangle|^2$, which satisfies the nonlinear

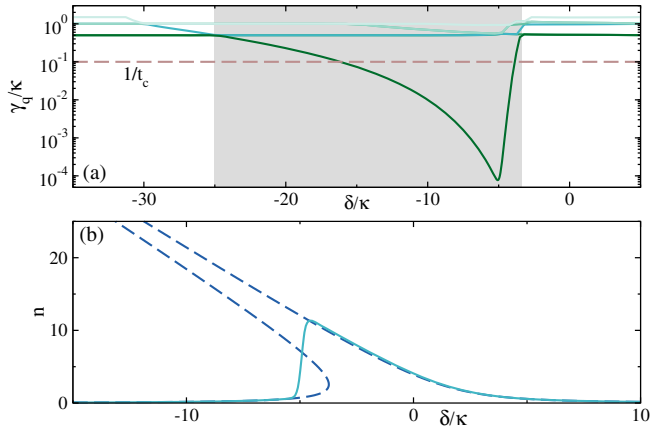

FIG. 2. (a) γ_q for few values of q. (Dashed line) $t_c = 10/\kappa$ is the duration of a step used in a staircase protocol sketched in Figs. 3(a) and 3(b). Gray area indicates the critical region of the width $\approx 21.8\kappa$. (b) (Solid line) The cavity occupation number $n = \langle b^\dagger b \rangle$ for the quantum steady state vs detuning δ. (Dashed lines) The mean-field solution $|\langle b \rangle|^2$ shown in the same range of δ. The parameter values $U = -0.5$ and $F = 4$ in the units of κ.

algebraic equation $|\beta_{ss}|^2(|\beta_{ss}|^2-\delta/U)^2+|\beta_{ss}|^2(\kappa/2U)^2=F^2/U^2$, is multivalued (the so-called optical bistability [26]). As a result, its shape considerably deviates from that of its quantum counterpart $n=\mathrm{tr}[b^\dagger b\rho_{ss}]$ (mostly in the critical regime of the control parameter δ) which is always unique [see Fig. 2(b)], but in the effective thermodynamic limit it is characterized by an infinite slope of the transition line between two different branches [29,36]. In general, such a discrepancy between quantum and semiclassical solutions signals the breakdown of a mean-field description.

In this regard, it becomes necessary to reconcile a semiclassical description of the critical multistable behavior in a nonlinear model, which is very efficient in predicting hysteretic effects seen in various experiments (see, e.g., [33,37]) and the Liouvillian description of the same system which, on one hand, captures quantum fluctuations and, on the other hand, predicts a unique steady state solution in generic models. In Refs. [35,38], it was proposed that the hysteresis in Markovian models can be *dynamically* simulated by a time-periodic change of the system's parameters with the appropriately chosen parameter ramp velocity [35] or modulation frequency [38]. Such a dynamical hysteresis has been recently observed experimentally [39].

Here we show how a complete reconciliation of semiclassical and Liouvillian ways of describing critical phenomena in open quantum systems is naturally achieved by introducing into the theory of additional timescales characterizing a typical duration of an experiment and other scales associated with parameter ramps and measurement protocols. In particular, we introduce the timescale t_c, which is preset as the waiting time between two successive parameter changes. In the parameter regime close to the driven DPT, where a clear separation $\gamma_1 \ll \gamma_{q\geq 2}$ of the relaxation rates takes place, it is meaningful to choose t_c in such a way that $\gamma_1 \ll 1/t_c \ll \gamma_{q\geq 2}$, as shown in Fig. 2(a). Choosing the quantum steady state as the initial condition just at the entrance $\delta_{\min}$ to the critical region (left edge of the gray area [40]), we consider the first experimental run by abruptly changing the control parameter to the value $\delta_{\min}+\Delta\delta$ and letting the system evolve during the time t_c [41]. After that the system's observables are being measured in the *metastable* state $|\rho^{\mathrm{ms}}_{\delta_{\min}+\Delta\delta}\rangle \approx |\rho^0_{\delta_{\min}+\Delta\delta}\rangle + |\rho^1_{\delta_{\min}+\Delta\delta}\rangle e^{-t_c\gamma_1(\delta_{\min}+\Delta\delta)}(\bar{\rho}^1_{\delta_{\min}+\Delta\delta}|\rho^0_{\delta_{\min}}\rangle)$ [42]. Repeating this procedure N times, where the number N should be large enough to reach the right edge of the critical region at $\delta_{\max}$ [see Fig. 2(a)], we relate the system's metastable states at successive $(k-1)$th and kth stages of the experiment by the recursive expression $|\rho^{\mathrm{ms}}_{\delta_k}\rangle \approx |\rho^0_{\delta_k}\rangle + |\rho^1_{\delta_k}\rangle e^{-t_c\gamma_1(\delta_k)}(\bar{\rho}^1_{\delta_k}|\rho^{\mathrm{ms}}_{\delta_{k-1}}\rangle)$, with $\delta_k=\delta_{\min}+k\Delta\delta$ and $1\leq k\leq N$. Taking the observable of interest $\hat{O}$, we collect the dataset of values $O_k=\mathrm{tr}[\hat{O}\rho^{\mathrm{ms}}_{\delta_k}]$, which are depicted in Figs. 3(c) and 3(d) by circles.

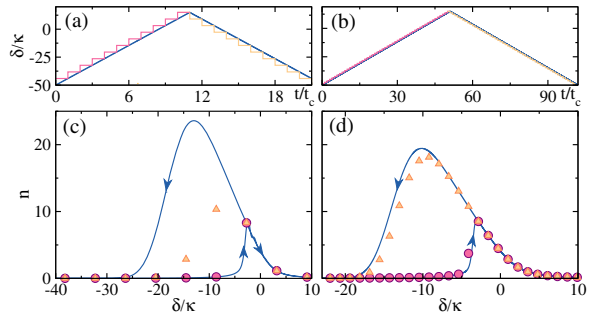

FIG. 3. Hysteretic behavior of the cavity occupation number n [(c),(d)] under sweeping the detuning parameter δ through the critical region in a stepwise manner or using a linear ramp with the same inclination [(a),(b)]. The duration of steps used in the former protocol is always the same, $t_c=10/\kappa$ [see also the dashed line in Fig. 2(a)]. [Filled circles (triangles)] Values of n calculated at multiples of t_c at which δ abruptly changes for a forward (backward) sweep. (Blue lines) Corresponding numerical results for the linear ramp with arrows indicating the sweep direction. The number of steps used in the calculations for the forward and backward sweep was taken to be $N=11$ [(a),(c)] and $N=51$ [(b),(d)]. The values of κ, U, and F are the same as those used in Fig. 2.

Analogously, we start from the value $\delta_{\max}$ and perform the same procedure with descending values $\delta'_k=\delta_{\max}-k\Delta\delta$. A sequence of metastable states along the reversed path in the one-dimensional parameter space is, however, different from the earlier obtained direct-path sequence even for the same values of δ. Hence, the observables are also different; see again Figs. 3(c) and 3(d), where the reversed-path observable values are depicted by triangles. Although both discrete datasets are obtained with the help of the same recursive expression, the difference between them arises due to the fact that in the first case the recursion is progressive, while in the second case it is regressive. So, the hysteretic behavior of observables in a typical experimental procedure is retrieved from the nonzero Liouvillian mode γ_1, which is responsible for the system's dynamics rather than for its steady state.

Comparing with each other the states $|\rho^{\mathrm{ms},\pm}_\delta\rangle = |\rho^0_\delta\rangle + \chi^\pm_\delta|\rho^1_\delta\rangle$, corresponding to the same value of δ and obtained from the ascending (sign "+") and descending (sign "−") staircase ramping protocols shown in Figs. 3(a) and 3(b), we notice that the real-valued coefficients χ^+_δ and χ^-_δ depend on a gauge choice. The gauge freedom in the present setting is provided [16–18] by a possibility to simultaneously rescale the left $(\bar{\rho}^q_\delta| \to (1/g_{q,\delta})(\bar{\rho}^q_\delta|$ and the right $|\rho^q_\delta) \to g_{q,\delta}|\rho^q_\delta)$ Liouvillian eigenvectors with $q\geq 1$ by the reciprocal real-valued coefficients. These transformations leave invariant the biorthogonality relations. For $q=0$, this freedom is not provided, since the rescaling of $(\bar{\rho}^0|$ is forbidden by the trace preservation; for this reason, the coefficient in front of $|\rho^0_\delta)$ in the above linear superposition is always fixed at the constant unit value,

which reflects the fundamental impossibility to acquire any geometric effects as well as hysteretic phenomena in unique steady state [18]. The gauge invariance of observables dictates the accompanying gauge transformation law $\chi_\delta^\pm \to (1/g_{1,\delta})\chi_\delta^\pm$, which renders the ratio $\chi_\delta^-/\chi_\delta^+$ manifestly gauge invariant.

It is more transparent to discuss the properties of $\chi_\delta^\pm$ in the continuum limit. Keeping t_c fixed, we reduce the discrete step $\Delta\delta$, and therefore we need to perform more steps to reach the value $\delta_{\max}$. Since the width of the critical area $(\delta_{\max}-\delta_{\min})$ is also fixed, the increment of N means diminishing of a ramp velocity $v=\Delta\delta/t_c=(\delta_{\max}-\delta_{\min})/(Nt_c)$. We notice that at sufficiently large $N\sim 50$ the difference between the staircase and the straightly linear [blue line in Figs. 3(a) and 3(b)] protocols begins to disappear: The deviation of circles and triangles collected during the staircase ramp from the continuous blue curve, which is obtained by a brute-force numerical integration of the time-dependent master equation with the linear ramp in the spirit of Ref. [35], becomes smaller and smaller with increasing value of N [compare Figs. 3(c) and 3(d)].

An effective geometric description of the continuum limit $\Delta\delta\to 0$ in our system featuring the driven DPT is achieved in terms of the ordinary differential equations for the gauge-invariant quantities $y^\pm(\delta)=\chi^\pm(\delta)/A_{10}(\delta)$ (see Supplemental Material [43] for details)

$$\frac{d}{d\delta}y^\pm(\delta)=-1-\left(f(\delta)\pm\frac{\gamma_1(\delta)}{v}\right)y^\pm(\delta), \qquad (1)$$

expressed in terms of the gauge-invariant function $f(\delta)=A_{11}(\delta)+(d/d\delta)\ln A_{10}(\delta)$ [see Fig. 4(a)] and equipped with initial conditions $y^+(\delta_{\min})=y^-(\delta_{\max})=0$. Note that all details about the driving protocol are now hidden in a value of the ramp velocity v, which acquires the meaning of a global characteristic in this limit being defined as $v=(\delta_{\max}-\delta_{\min})/(Nt_c)$. This indicates that all results of Eq. (1) remain robust to any experimental imperfections of a driving protocol.

The Sarandy-Lidar connections $A_{q'q}(\delta)=(\bar\rho^{q'}(\delta)|d/d\delta|\rho^q(\delta))$ entering this equation are the geometric objects obtained from a solution of the instantaneous Liouvillian eigenvalue problem, in close analogy to the derivation of the Berry connection. It should be stressed that $A_{q'q}(\delta)$ can be unambiguously extracted from measurements by performing the forward and backward sweeping; see Supplemental Material [43] for details. The term $\propto v^{-1}$ in Eq. (1) is the open system analog of the dynamical phase in closed systems. The sign difference in this equation determines the hysteresis effect in the continuum limit: Experimentally, the best candidate to probe geometric effects in open systems is a hysteresis area $\mathcal{A}=\int_{\delta_{\min}}^{\delta_{\max}}d\delta[\chi^-(\delta)-\chi^+(\delta)]$ (here expressed in the *observable* gauge fixed by the condition $\mathrm{tr}[\hat O\rho_\delta^1]=1$) for the expectation value of an observable $\hat O$ obtained under a cyclic variation of control parameters; see the insets in Fig. 4(b) for typical results.

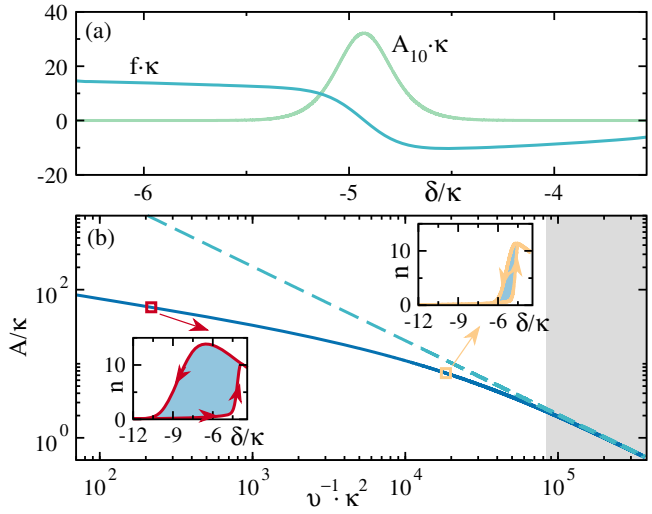

FIG. 4. (a) Sarandy-Lidar geometrical connection $A_{10}(\delta)$ in the gauge $\mathrm{tr}[b^\dagger b\rho_1(\delta)]=1$ and the gauge-invariant function $f(\delta)$. (b) Hysteretic area $\mathcal{A}$ (solid line) as a function of v^{-1}. (Insets) The cavity occupation number n of the metastable states for the staircase protocol [see Figs. 3(a) and 3(b)] with the number of steps $N\approx 1.4\times 10^3$ (left inset) and $N\approx 1.2\times 10^5$ (right inset) in either direction. (Dashed line) Quasiadiabatic approximation for $\mathcal{A}\propto v$ becomes valid only for extremely slow sweeping velocities (gray region).

Equation (1) can be cast to the matrix form [43] revealing the non-Abelian character of this open system geometric effect. For this reason, it is impossible to fully separate geometric and dynamical contributions to $\chi^\pm$. We also note that the non-Abelian description provided here is substantially different from the one considered in Refs. [16,17], because in our case there is no degeneracy between $\lambda_0=0$ and $\lambda_1=-i\gamma_1$ Liouvillian eigenvalues. The absence of degeneracy prevents a cancellation of contributions to the hysteresis area accumulated in the forward and backward integration directions. This essential property, together with the relaxation rate's separation near the DPT, allows us to introduce the effective geometric description of the open system metastable dynamics even in the one-dimensional parameter space—the property, which is absent in a geometric description of closed adiabatic dynamics.

Yet another advantage of the description in terms of Eq. (1) is a numerically cheap study of slow and ultraslow ramps, for which a brute-force numerical study becomes very expensive. One just needs to store the values of $A_{10}(\delta)$ and $A_{11}(\delta)$ in some (e.g., observable) gauge shown in Fig. 4(a) (with $\hat O=b^\dagger b$) along with the gauge-independent function $\gamma_1(\delta)$ shown in Fig. 2(a), and solve the ordinary differential equations (1) with arbitrary small values of v. Thereby it is easy to obtain the scaling behavior of the hysteresis areas covering a range of sweep velocities v within many orders of magnitude [see Fig. 4(b)].

Remarkably, the quantities defining $\chi^{\pm}(\delta)$ can be extracted from a realistic experiment. To this end, one needs to perform measurements at three different values of v in the forward and backward directions: This suffices to find $\gamma_1(\delta)$, $A_{10}(\delta)$, and $f(\delta)$ inside the critical region (see Supplemental Material [43]).

At ultraslow v [for the parameters of Fig. 4(b), this corresponds to $N \sim 10^6$], the dynamical term in Eq. (1) dominates, allowing us to find the asymptotic formula $\chi^{\pm}(\delta) = \mp vA_{10}(\delta)/\gamma_1(\delta) + O(v^2)$. Thereby we recover the quasiadiabatic phase of Landsberg [44] and Ning and Haken [45], which is also known from two-parameter pumping problems [18,21]. This formula suggests that the scaling of the hysteresis areas is asymptotically linear at small v (cf. [35]; see also [46]). We also find the universal relation $\chi^{-}(\delta)/\chi^{+}(\delta) = -1$ in this regime.

In summary, we provided the geometric description of the metastable dynamics of the open quantum system close to DPT and proposed the way to determine the components of the Berry-like (Sarandy-Lidar) connections necessary for this purpose in a real experiment. Experimentally, our general approach can be implemented in modern hybrid quantum systems [47,48] based on various physical realizations, such as qubits, mesoscopic spin ensembles, and quantum metamaterials disposed on a single chip or in Rydberg systems [49].

We are grateful to Maarten Wegewijs for enlightening discussions. M. P. acknowledges financial support by the Deutsche Forschungsgemeinschaft via RTG 1995. Some of the computational results presented here have been achieved using the Vienna Scientific Cluster (VSC).

*dmitry.krimer@gmail.com
†pletmikh@physik.rwth-aachen.de

[1] M. V. Berry, Quantal phase factors accompanying adiabatic changes, Proc. R. Soc. A **392**, 45 (1984).
[2] M. V. Berry, The quantum phase, five years after, in *Geometric Phases in Physics*, Advanced Series in Mathematical Physics Vol. 5, edited by A. Shapere and F. Wilczek (World Scientific, Singapore, 1989).
[3] B. Simon, Holonomy, the Quantum Adiabatic Theorem, and Berry's Phase, Phys. Rev. Lett. **51**, 2167 (1983).
[4] A. Altland and M. R. Zirnbauer, Nonstandard symmetry classes in mesoscopic normal-superconducting hybrid structures, Phys. Rev. B **55**, 1142 (1997).
[5] S. Ryu, A. Schnyder, A. Furusaki, and A. Ludwig, Topological insulators and superconductors: Tenfold way and dimensional hierarchy, New J. Phys. **12**, 065010 (2010).
[6] M. Z. Hasan and C. L. Kane, Colloquium: Topological insulators, Rev. Mod. Phys. **82**, 3045 (2010).
[7] X.-L. Qi and S.-C. Zhang, Topological insulators and superconductors, Rev. Mod. Phys. **83**, 1057 (2011).
[8] T. Schulz, R. Ritz, A. Bauer, M. Halder, M. Wagner, C. Franz, C. Pfleiderer, K. Everschor, M. Garst, and A. Rosch, Emergent electrodynamics of skyrmions in a chiral magnet, Nat. Phys. **8**, 301 (2012).
[9] H. B. Braun, Topological effects in nanomagnetism: From superparamagnetism to chiral quantum solitons, Adv. Phys. **61**, 1 (2012).
[10] K. von Bergmann, A. Kubetzka, O. Pietzsch, and R. Wiesendanger, Interface-induced chiral domain walls, spin spirals and skyrmions revealed by spin-polarized scanning tunneling microscopy, J. Phys. Condens. Matter **26**, 394002 (2014).
[11] Z. Wang, Y. Chong, J. D. Joannopoulos, and M. Soljacic, Observation of unidirectional backscattering-immune topological electromagnetic states, Nature (London) **461**, 772 (2009).
[12] M. Hafezi, S. Mittal, J. Fan, A. Migdall, and J. M. Taylor, Imaging topological edge states in silicon photonics, Nat. Photonics **7**, 1001 (2013).
[13] L. Lu, J. D. Joannopoulos, and M. Soljacic, Topological photonics, Nat. Photonics **8**, 821 (2014).
[14] M. Eichenfield, J. Chan, R. M. Camacho, K. J. Vahala, and O. Painter, Optomechanical crystals, Nature (London) **462**, 78 (2009).
[15] A. H. Safavi-Naeini, J. T. Hill, S. Meenehan, J. Chan, S. Gröblacher, and O. Painter, Two-Dimensional Phononic-Photonic Band Gap Optomechanical Crystal Cavity, Phys. Rev. Lett. **112**, 153603 (2014).
[16] M. S. Sarandy and D. A. Lidar, Adiabatic approximation in open quantum systems, Phys. Rev. A **71**, 012331 (2005).
[17] M. S. Sarandy and D. A. Lidar, Abelian and non-Abelian geometric phases in adiabatic open quantum systems, Phys. Rev. A **73**, 062101 (2006).
[18] T. Pluecker, M. R. Wegewijs, and J. Splettstoesser, Gauge freedom in observables and Landsberg's nonadiabatic geometric phase: Pumping spectroscopy of interacting open quantum systems, Phys. Rev. B **95**, 155431 (2017).
[19] J. E. Avron, M. Fraas, and G. M. Graf, Adiabatic response for Lindblad dynamics, J. Stat. Phys. **148**, 800 (2012).
[20] V. V. Albert, B. Bradlyn, M. Fraas, and L. Jiang, Geometry and Response of Lindbladians, Phys. Rev. X **6**, 041031 (2016).
[21] F. Reckermann, J. Splettstoesser, and M. R. Wegewijs, Interaction-Induced Adiabatic Nonlinear Transport, Phys. Rev. Lett. **104**, 226803 (2010).
[22] S. Diehl, E. Rico, M. A. Baranov, and P. Zoller, Topology by dissipation in atomic quantum wires, Nat. Phys. **7**, 971 (2011).
[23] T. J. Milburn, J. Doppler, C. A. Holmes, S. Portolan, S. Rotter, and P. Rabl, General description of quasiadiabatic dynamical phenomena near exceptional points, Phys. Rev. A **92**, 052124 (2015).
[24] J. Doppler, A. A. Mailybaev, J. Böhm, U. Kuhl, A. Girschik, F. Libisch, T. J. Milburn, P. Rabl, N. Moiseyev, and S. Rotter, Dynamically encircling an exceptional point for asymmetric mode switching, Nature (London) **537**, 76 (2016).
[25] H. J. Carmichael, Breakdown of Photon Blockade: A Dissipative Quantum Phase Transition in Zero Dimensions, Phys. Rev. X **5**, 031028 (2015).

[26] P. D. Drummond and D. F. Walls, Quantum theory of optical bistability. I: Nonlinear polarisability model, J. Phys. A **13**, 725 (1980).
[27] A. Le Boité, M.-J. Hwang, and M. B. Plenio, Metastability in the driven-dissipative Rabi model, Phys. Rev. A **95**, 023829 (2017).
[28] K. Macieszczak, M. Guta, I. Lesanovsky, and J. P. Garrahan, Towards a Theory of Metastability in Open Quantum Dynamics, Phys. Rev. Lett. **116**, 240404 (2016).
[29] F. Minganti, A. Biella, N. Bartolo, and C. Ciuti, Spectral theory of Liouvillians for dissipative phase transitions, Phys. Rev. A **98**, 042118 (2018).
[30] M. A. Armen and H. Mabuchi, Low-lying bifurcations in cavity quantum electrodynamics, Phys. Rev. A **73**, 063801 (2006).
[31] V. E. Manucharyan, E. Boaknin, M. Metcalfe, R. Vijay, I. Siddiqi, and M. Devoret, Microwave bifurcation of a Josephson junction: Embedding-circuit requirements, Phys. Rev. B **76**, 014524 (2007).
[32] W. Wustmann and V. Shumeiko, Parametric resonance in tunable superconducting cavities, Phys. Rev. B **87**, 184501 (2013).
[33] A. Angerer, S. Putz, D. O. Krimer, T. Astner, M. Zens, R. Glattauer, K. Streltsov, W. J. Munro, K. Nemoto, S. Rotter, J. Schmiedmayer, and J. Majer, Dynamical exploration of amplitude bistability in engineered quantum systems, Sci. Adv. **3**, e1701626 (2017).
[34] D. O. Krimer, M. Zens, and S. Rotter, Critical phenomena and nonlinear dynamics in a spin ensemble strongly coupled to a cavity. I. Semiclassical approach, Phys. Rev. A **100**, 013855 (2019).
[35] W. Casteels, F. Storme, A. Le Boité, and C. Ciuti, Power laws in the dynamic hysteresis of quantum nonlinear photonic resonators, Phys. Rev. A **93**, 033824 (2016).
[36] W. Casteels, R. Fazio, and C. Ciuti, Critical dynamical properties of a first-order dissipative phase transition, Phys. Rev. A **95**, 012128 (2017).
[37] I. Siddiqi, R. Vijay, F. Pierre, C. M. Wilson, M. Metcalfe, C. Rigetti, L. Frunzio, and M. H. Devoret, RF-Driven Josephson Bifurcation Amplifier for Quantum Measurement, Phys. Rev. Lett. **93**, 207002 (2004).
[38] V. Reimer, K. Pedersen, N. Tanger, M. Pletyukhov, and V. Gritsev, Nonadiabatic effects in periodically driven dissipative open quantum systems, Phys. Rev. A **97**, 043851 (2018).
[39] S. R. K. Rodriguez, W. Casteels, F. Storme, N. Carlon Zambon, I. Sagnes, L. Le Gratiet, E. Galopin, A. Lemaitre, A. Amo, C. Ciuti, and J. Bloch, Probing a Dissipative Phase Transition Via Dynamical Optical Hysteresis, Phys. Rev. Lett. **118**, 247402 (2017).
[40] We call the regime noncritical whenever $1/t_c \ll \gamma_{q\geq 1}$.
[41] Without loss of generality, we assume that $|\rho(t=0)) = |\rho^0_{\delta_{\min}})$.
[42] A truncation of the higher Liouvillian modes with $q \geq 2$ relying on the condition $e^{-t_c\gamma_q} \ll 1$ provides a description of metastable states in terms of just two Liouvillian modes $|\rho^0)$ and $|\rho^1)$. Additionally, we note that ω_1 identically vanishes in the critical regime, see [35].
[43] See Supplemental Material at http://link.aps.org/supplemental/10.1103/PhysRevLett.123.110604 where we briefly sketch the derivation of the master equation and the eigenvalue problem, present details on a simplified description of metastable states and explain how the connection components can be experimentally extracted. The results of calculations on sweeping the pumping field amplitude are also discussed.
[44] A. S. Landsberg, Geometrical Phases and Symmetries in Dissipative Systems, Phys. Rev. Lett. **69**, 865 (1992).
[45] C. Z. Ning and H. Haken, Geometrical Phase and Amplitude Accumulations in Dissipative Systems with Cyclic Attractors, Phys. Rev. Lett. **68**, 2109 (1992).
[46] It is worth noting that sweeping the drive amplitude F at a fixed value of δ not only leads to a much weaker closure of the Liouvillian gap, but also leads to the undesirable effect of nonvanishing entropy outside the critical region as compared to the case when the detuning parameter δ is swept. As a consequence, geometrical effects related to the hysteretic area become much less pronounced (see also Supplemental Material [43] for more details).
[47] Z.-L. Xiang, S. Ashhab, J. Q. You, and F. Nori, Hybrid quantum circuits: Superconducting circuits interacting with other quantum systems, Rev. Mod. Phys. **85**, 623 (2013).
[48] G. Kurizki, P. Bertet, Y. Kubo, K. Mølmer, D. Petrosyan, P. Rabl, and J. Schmiedmayer, Quantum technologies with hybrid systems, Proc. Natl. Acad. Sci. U.S.A. **112**, 3866 (2015).
[49] F. Letscher, O. Thomas, T. Niederprüm, M. Fleischhauer, and H. Ott, Bistability Versus Metastability in Driven Dissipative Rydberg Gases, Phys. Rev. X **7**, 021020 (2017).